Distinctive sedimentary processes on two contrasting tidal flats of the Yellow River Delta

Xie, Weiming; Sun, Jianwei; Guo, Leicheng; Xu, Fan; Wang, Xianye; Ji, Hongyu; Fan, Yaoshen; Wang, Zheng bing ; He, Qing

DOI
10.3389/fmars.2023.1259081

Publication date
2023

Document Version
Final published version

Published in
Frontiers in Marine Science

frontiers | Frontiers in Marine Science

TYPE Original Research
PUBLISHED 25 August 2023
DOI 10.3389/fmars.2023.1259081

OPEN ACCESS

EDITED BY
Shunqi Pan,
Cardiff University, United Kingdom

REVIEWED BY
Boyuan Zhu,
Changsha University of Science and Technology, China
Feng Liu,
Sun Yat-sen University, China

*CORRESPONDENCE
Jianwei Sun
J.Sun-5@tudelft.nl
Xianye Wang
xywang@sklec.ecnu.edu.cn

RECEIVED 15 July 2023
ACCEPTED 08 August 2023
PUBLISHED 25 August 2023

CITATION
Xie W, Sun J, Guo L, Xu F, Wang X, Ji H, Fan Y, Wang ZB and He Q (2023) Distinctive sedimentary processes on two contrasting tidal flats of the Yellow River Delta.
Front. Mar. Sci. 10:1259081.
doi: 10.3389/fmars.2023.1259081

Distinctive sedimentary processes on two contrasting tidal flats of the Yellow River Delta

Weiming Xie[1], Jianwei Sun[2*], Leicheng Guo[1], Fan Xu[1], Xianye Wang[1*], Hongyu Ji[1], Yaoshen Fan[3], Zheng Bing Wang[2,4] and Qing He[1]

[1]State Key Laboratory of Estuarine and Coastal Research, East China Normal University, Shanghai, China, [2]Faculty of Civil Engineering and Geosciences, Delft University of Technology, Delft, Netherlands, [3]Yellow River Institute of Hydraulic Research, Yellow River Conservancy Commission, Zhengzhou, China, [4]Deltares, Delft, Netherlands

Coastal tidal flats provide valuable ecosystems, but are highly sensitive to tidal dynamics, sea-level rise, and human activities. Tidal inundation depth and frequency are known to affect tidal flat morphodynamics. However, the causes, processes and extent remain uncertain, particularly given the associated changes in sediment availability. In this study, we monitored the hydrodynamics, sediment transport, and morphological changes on two tidal flats in the northern and southern parts of the Yellow River Delta, with contrasting tidal regimes. The data showed that longer inundation periods under diurnal tides gained additional sediment and deposition than under semi-diurnal tides, because of the associated increase in water depth and sediment availability. The wave impact increased at the site with a semi-diurnal tidal regime owing to the lower water depth, where a larger bed shear stress led to tidal flat erosion. These results indicated that the combination of tidal regime and the occurrence of powerful waves played a joint role in controlling bed erosion, sediment availability, and short-term tidal flat evolution. This has implications for coping with delta erosion by enhancing local sediment availability in diurnal tidal regions and restoring vegetation to attenuate waves in semi-diurnal regions of the Yellow River Delta.

KEYWORDS

tidal flat, hydrodynamics, sediment dynamics, inundation period, Yellow River Delta

1 Introduction

Estuarine and coastal tidal flats host important ecosystems, such as habitats necessary for migrating birds (Kirwan and Megonigal, 2013; Temmerman et al., 2013). Currently, tidal flats are facing increasing pressure owing to changes in forcing conditions, sea-level rise, and human modifications. The decline in fluvial sediment supply plays a vital role in

inducing river delta erosion and tidal flat retreat (Syvitski et al., 2009). Accelerating sea-level rise further exacerbates delta erosion and the loss of tidal flats (Bouma et al., 2016; IPCC, 2021). Human activities, such as the construction of coastal seawalls and dykes, change the regional hydrodynamics and sediment transport, exerting strong impacts on tidal flat evolution (van der Wal and Pye, 2004; Xie et al., 2018b; Liu et al., 2022). Understanding the sedimentary processes of tidal flats is essential from a coastal protection and management perspective. However, it remains challenging to determine short- to long-term tidal flat morphodynamics that involve the interaction of several factors, such as sediment supply, tidal conditions, currents, waves, vegetation, sea-level rise, and storms (Allen, 2000; Friedrichs, 2011; D'Alpaos and Marani, 2016).

Tidal flat sedimentary processes and their controlling mechanisms vary in different estuarine environments. The fluvial sediment supply is a key factor in estuarine tidal flat evolution (Yang et al., 2011b; Blum and Roberts, 2012; Zhu et al., 2019). A time lag between changes in fluvial sediment supply and delta morphodynamic response was identified in the Changjiang Delta, which was ascribed to the delta's inherent morphodynamic buffering capacity (Zhu et al., 2019). The fluvial sediment supply also controls regional sediment availability, which directly influences medium-scale tidal flat evolution (Maan et al., 2019). Moreover, waves have a strong impact on tidal flat evolution by simulating erosion and developing a concave-up profile (van Rijn, 1993; Green and Coco, 2014; Gao et al., 2020). Wave-induced sediment resuspension, combined with sediment transport by currents, determines the sedimentary processes of tidal flats. Waves also control river channel orientation and delta aggradation through wave-induced bypassing of sediment flux (Nienhuis et al., 2016; Gao et al., 2020). Sea level rise has accelerated in the past century and is expected to enhance coastal erosion and the loss of estuarine tidal flats (van der Wegen, 2013; Leuven et al., 2019). It is projected that tidal flat accretion may not keep pace with the rise in sea level and is likely to be flooded (Spencer et al., 2016; Maan et al., 2019). In exceptional cases, tidal flats might survive a low rise in the sea level with sediment supply or import from coasts, for example, in the Dutch Wadden Sea (Wang et al., 2018). Furthermore, vegetation can attenuate wave energy and trap suspended sediment on tidal flats, although sediment trapping efficiency is a function of plant species, growth, and biomass (Temmerman et al., 2005; Bouma et al., 2009; Li and Yang, 2009). Extreme events such as storms, associated strong wave activities, and high bed shear stresses also play a vital role in tidal flat evolution, particularly in causing tidal flat erosion (Mariotti et al., 2010; Xie et al., 2017).

In addition to the dynamic variability in different deltas and estuaries, the sedimentary dynamics in different parts of the same river delta may also vary, owing to changes in the coastal landscape and distinctive sheltering. This regional variability can induce different hydro-morphodynamic behaviors. For instance, Nienhuis et al. (2016) observed that waves led to the asymmetric evolution of deltas such as Ombrone in Italy and Danube in Romania. Flow asymmetry and sediment composition are also considered dominant factors in the evolution of deltas (Mariotti and Fagherazzi, 2011; van Maren and Winterwerp, 2013). The difference in local sediment availability was found to have a strong impact on the asymmetry of the tidal flat evolution (Stammermann and Piasecki, 2012; Xie et al., 2018b). However, the way in which primary tidal forcing can induce asymmetric sedimentary dynamics within the same delta remains uncertain.

The Yellow River Delta faces the most severe risk among deltas worldwide (Syvitski et al., 2009). To determine representative sites for our study, we observe that the tidal regime around the Yellow River Delta in China exhibits large spatial variations. The northern part of the delta has a diurnal tidal regime, whereas the southern part is predominantly a mixed semidiurnal tide (Ji et al., 2020). The morphodynamic evolution of the northern and southern parts of the Yellow River Delta also exhibits different behaviors, rendering it an ideal location for the study of asymmetric tidal flat morphodynamics. The current understanding of how different tidal regimes affect sediment transport and erosion-deposition patterns is insufficient.

This study aimed at highlighting the profound hydro-morphodynamic effect of tidal condition on the contrasting tidal flat evolution, which shed lights on coastal protection and management. Therefore, we conducted field measurements of currents, waves, suspended sediment concentration, and bed level changes in two regions of the Yellow River Delta. The two main aims of the study were to determine (1) how differences in water motion and sediment transport influence sedimentary processes and (2) whether different types of tides are the determining factors in controlling asymmetric tidal flat evolution.

2 Methods

2.1 Study area

The modern Yellow River Delta is a river-dominated system that started forming in 1855, at that time the Yellow River entered the Bohai Sea (Figure 1). In the past 170 years, a fan-shaped delta has taken shape owing to frequent channel avulsion. The current active Yellow River Delta lobe started to develop in 1976, when the previous active channel toward the north was abandoned (Wang et al., 2017). The river channel avulsed again in 1996, shifting north (Figure 1).

The Yellow River Delta is dominated by micro-tidal tides with a mean range of 0.73–1.77 m (Yang et al., 2011a). Spatially, the northern part of the present delta lobe has a diurnal tidal regime, whereas the southern region has a mixed semi-diurnal tidal regime (Ji et al., 2020). Field observations were conducted on the northern Qingshuigou tidal flat (QSG) and southern Kendong-dyke tidal flat (KDD) (Figure 1). The elevation was approximately −0.2 m above mean sea level for both (Figures 1C, D). The tidal flat profiles were convex-up at the QSG site and concave-up at the KDD site (Figure 1). The surface sediments were composed of silt and sand with median diameters of ~60 μm and ~66 μm at the QSG and KDD, respectively (Figure 2). The two sites were submerged during high tides, with a maximum water depth of 0.9 m, but exposed during low tides. Both tidal flats were bare and without vegetation (Figure 3A).

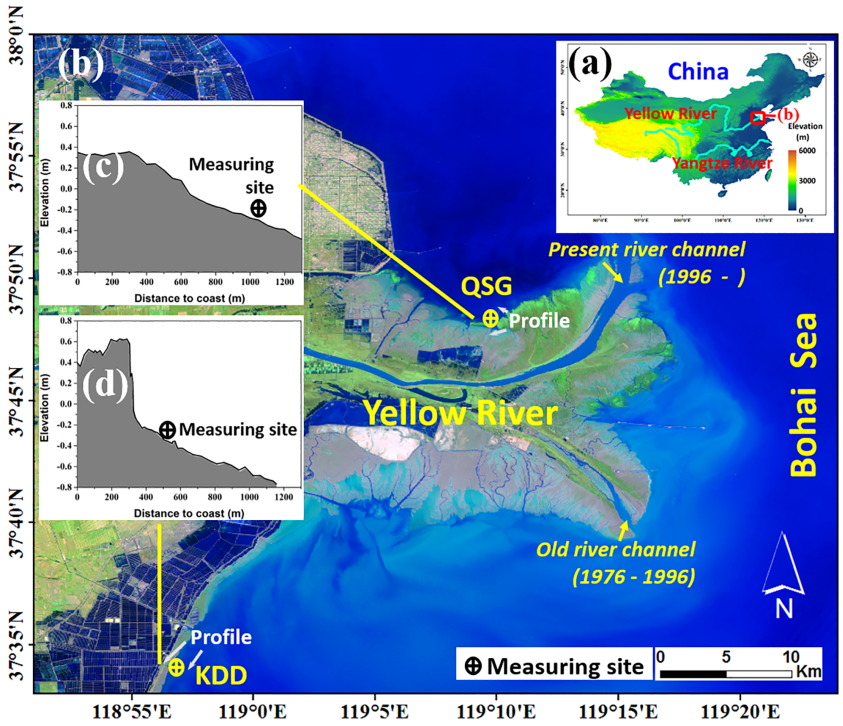

FIGURE 1
Locations of **(A)** the Yellow River Delta and **(B)** the two studied sites, **(C)** the elevation profile of the QSG site and **(D)** the elevation profile of the KDD site. The locations of the two measuring sites are also marked on the profiles.

2.2 Field measurements

Hydrodynamic measurements were performed from 10:00 on November 19 to 10:00 on November 23, 2019. The fluvial sediment flux from the Yellow River, monitored at the Lijin Hydrometric Station, was low during this period (Figure 4). Thus, the direct influence of riverine sediment on tidal flat evolution in the study area may be negligible. Current velocity, suspended sediment concentration (SSC), wave activity, and bed-level changes were collected, using two tripod systems mounted on the bed of the two sites (Figure 3A). Both tripods were equipped with an acoustic doppler velocimeter (ADV) (Nortek AS, Norway), an optical backscattering sensor (OBS) (Campbell Scientific., USA), and a tide and wave logger (RBR) (RBR Limited, Canada). The ADVs, OBSs, and RBRs were placed 30 cm, 10 cm, and 10 cm above the bed surface, respectively. The ADVs were set up in 64 Hz mode, with a burst interval of 5 min recorded both the near-bed 3D velocity and bed-level change (Andersen et al., 2007; Zhu et al., 2016; Xie et al., 2018a). RBRs were deployed to measure the wave activity and water depth. The optical backscatter signal of the OBSs was used to estimate the SSC, with sampling every 5 min. The calibration of the optical backscatter signal into the SSC is shown in Figure 3B.

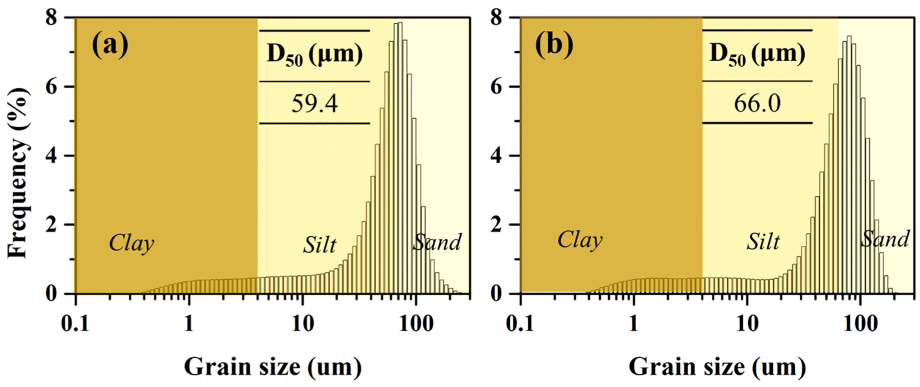

FIGURE 2
The composition of the surficial sediment and median diameter at **(A)** the QSG site and **(B)** the KDD site.

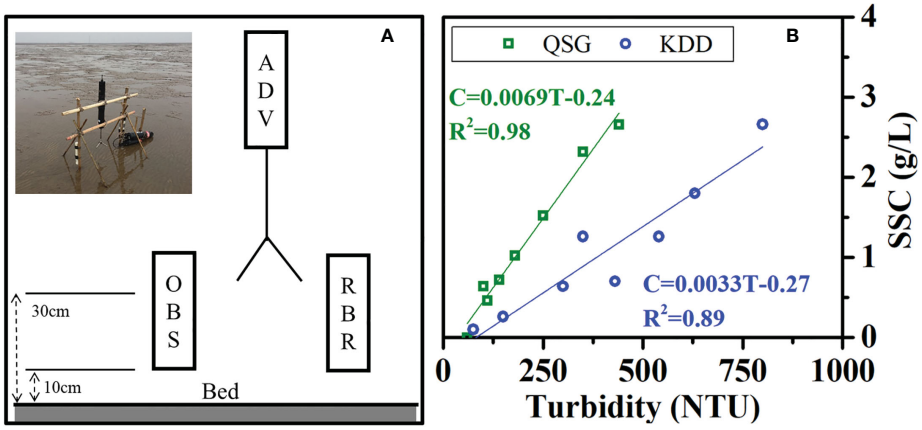

FIGURE 3
(A) Field measuring tripod and the location of the ADV, OBS, and RBR, and **(B)** calibration of the optical backscatter signal with SSC data at the two sites.

2.3 Calculation of bed shear stress on tidal flats

Field estimations of the current-induced and wave-induced bed shear stresses are made using ADV and RBR. These estimates are useful for understanding sediment dynamics and sedimentary processes *in situ* using tidal currents and waves.

The measured current velocities (u, v, w) can be decomposed into terms of the mean (U, V, W) and fluctuating components (u', v', w'). Several studies have estimated the bed shear stress from the second components, including the prevalent turbulent kinetic energy (TKE) method, where the TKE (J/m^3) is estimated from the fluctuating components:

$$TKE = \frac{1}{2}\rho_w(u'^2 + v'^2 + w'^2) \quad (1)$$

Where ρ_w is the water density at 20°C (ρ = 1030 kg/m^3 in this study) (Andersen et al., 2007; Xie et al., 2018b),

The current-induced bed shear stress (τ_c, N/m^2) is estimated using:

$$\tau_c = C \times TKE \quad (2)$$

and C is a constant (C = 0.19) (Stapleton and Huntley, 1995; Pope et al., 2006).

Furthermore, the peak wave orbital velocity ($\hat{U}_\delta$) m/s) is related to the wave-induced bed shear stress (τ_w, N/m^2) by the wave friction coefficient f_w (van Rijn, 1993):

$$\tau_w = \frac{1}{4}\rho_w f_w \hat{U}_\delta^2 \quad (3)$$

where the peak wave orbital velocity ($\hat{U}_\delta$) and peak orbital excursion ($\hat{A}_\delta$)can be calculated using linear wave theory (Stokes, 1847):

$$\hat{U}_\delta = \omega\hat{A}_\delta = \frac{\pi H}{T sinh(kh)} \quad (4)$$

$$\hat{A}_\delta = \frac{H}{2sinh(kh)} \quad (5)$$

where H is the wave height (m), T is the wave period (s), h is the water depth (m), L is the wavelength (m) ($L = (gT^2/2\pi)tanh(kh)$), k

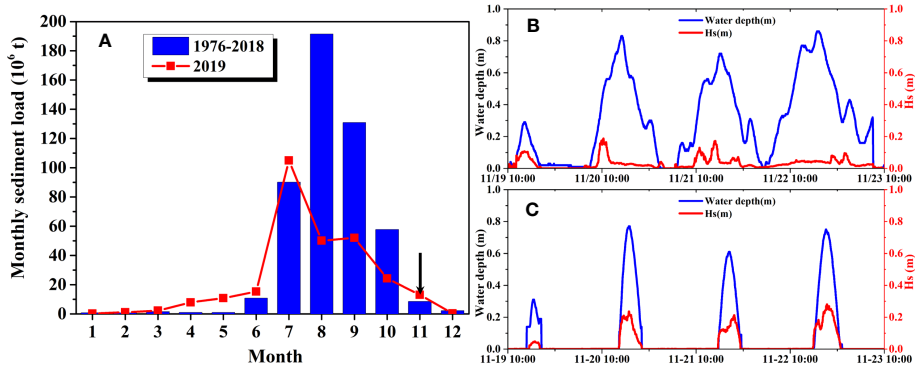

FIGURE 4
(A) Monthly average sediment load into the Yellow River Delta from 1976 to 2018 and in 2019, and time series of significant wave heights and water depths during the study period at **(B)** the QSG site and **(C)** the KDD site.

10.3389/fmars.2023.1259081

is the wave number ($k = 2\pi/L$), ω is the angular velocity (rad/s), and g is the gravitational acceleration (g = 9.8 m/s^2).

The wave friction coefficient (f_w) is determined by the hydraulic regime (Soulsby, 1997):

$$f_w = \begin{cases} 2Re_w^{-0.5}, & Re_w \le 10^5 \quad (laminar) \\ 0.0521Re_w^{-0.187}, & Re_w > 10^5 (smooth \quad turbulent) \\ 0.237r^{-0.52}, & (rough \quad turbulent) \end{cases} \quad (6)$$

Where Re_w is the wave Reynolds number ($Re_w = \frac{\hat{U}_\delta \hat{A}_\delta}{\nu}$), r is the relative roughness ($r = \frac{\hat{A}_\delta}{k_s}$), k_s is the Nikuradse roughness ($k_s = 2.5d_{50}$), d_{50} is the median diameter of the surficial sediment, and ν is the kinematic viscosity of water (ν = 1.5×10^{-6} m^2/s).

Then, the combined wave-current bed shear stress (τ_{cw}, N/m^2) can be estimated using the following hydrodynamic formulation (Soulsby, 1997):

$$\tau_{cw} = \tau_c \left[1 + 1.2 \left(\frac{\tau_w}{\tau_c + \tau_w} \right)^{3.2} \right] \quad (7)$$

Where τ_c is the current-generated bed shear stress, and τ_w is the wave-induced bed shear stress.

The root-mean-square value $\tau_{rms}$is a good average measure of the bed shear stress, particularly useful in random waves. So $\tau_{rms}$is used here to describe the bed shear stress and it can be estimated using the following hydrodynamic formulation (Soulsby and Clarke, 2005):

$$\tau_{rms} = \left(\tau_{cw}2 + \frac{1}{2}\tau_w 2 \right)^{1/2} \quad (8)$$

3 Results

3.1 Difference in the hydrodynamics

The Yellow River Delta is in a micro-tidal environment, and the tidal range was less than 1.0 m at both the QSG and KDD sites (Figures 4B and C). The inundation period at the QSG site was much longer than that at the KDD site. The QSG tidal flat was always submerged during the tidal cycle, whereas the KDD tidal flat was submerged for less than 7 h per day (Figures 5A, 6A).

Wave activities at the KDD site were stronger than those at the QSG site during the observation period (Figures 4B, C). The averaged significant wave height was 0.10 m at KDD while it was only 0.03 m at QSG. At the KDD site, the wave heights were higher when the tidal flats were submerged; however, this was not the case at the QSG site (Figures 4B, C). These differences were ascribed to different coastal landscapes: the QSG site was located in a sheltered bay, whereas the KDD site was open to the sea (Figure 1).

The ADV data indicated that the velocity in the vertical direction was always negligible compared to that in the horizontal direction. Therefore, we assumed that the current was two-dimensional. The current on the tidal flat was more complex than that of a simple bidirectional flow. For simplicity, the velocity was projected along two directions: the eastern direction (positive for the east) and northern direction (positive for the north). At the QSG site, which is parallel with the coast, the velocity component along the eastern direction was relatively small (< 0.05 m/s) (Figure 5B). During the flood period, the direction of the current was between 170°N and 210°N. During the ebb, it was between 330°N and 10°N. At the KDD site, the current direction during the flood and ebb periods was between 310°N and 10°N, and 100°N and 150°N, respectively (Figure 6B). The current direction was symmetric with respect to the highest water level at the KDD site (Figure 6B), whereas it showed no clear correlation with the tidal oscillation at the QSG site (Figure 5B).

For each tidal cycle, the current velocity, at both the QSG and KDD sites, was higher during the flood than during the ebb (Table 1). The average velocity at the QSG site was higher than at the KDD site. At the QSG site, the average velocity was 0.09 m/s for the tidal cycle. The velocity varied between 0.07 m/s and 0.16 m/s during the flood period, and between 0.08 m/s and 0.10 m/s during the ebb period. The maximum flood velocity occurred when the water depth was ~0.30 m, and the maximum ebb velocity occurred at a higher elevation of ~0.40 m (Figure 5B). The velocity decreased to zero in the slack water. At the KDD site, the velocity was relatively low (<0.07 m/s) for most of the tidal period. During the flood, the velocity ranged from 0.03–0.07 m/s. During the ebb, it was between 0.02 m/s and 0.03 m/s. The maximum flood velocity appeared at the beginning of the tidal cycle and then decreased to zero during high slack water (Figure 6B). The maximum ebb velocity was reached when the water depth was less than 0.20 m (Figure 6B).

There was strong fluctuation in the water level and velocity at the QSG site, indicating the currents flowed forward and back frequently at a short timescale (hours). By contrast, the currents were bidirectional flows at the KDD site.

3.2 Asymmetry in bed shear stress and sediment dynamics

The bed shear stress was calculated under the combined effect of waves (τ_c) and currents (τ_w) for both sites (Figures 5C, 6C). On average, the bed shear stress (τ_{rms}) at the QSG site (0.27 N/m^2) was much smaller than that at the KDD site (0.43 N/m^2) (Table 1). The wave-induced bed shear stress (τ_w) had a stronger influence on the KDD site than the sheltered QSG site. At the QSG site, the τ_c ranged from 0.01–0.61 N/m^2 with an average value of 0.10 N/m^2 and τ_w ranged from 0.03–0.85 N/m^2 with an average value of 0.20 N/m^2. The τ_{rms} showed weak correlation with tidal oscillations. At the KDD site, the average τ_w was high, reaching 0.64 N/m^2. The τ_c ranged from 0.01–0.30 N/m^2, with an average value of 0.07 N/m^2. In general, the τ_{rms} of the KDD site was higher during the flood period than during the ebb period. Peak τ_{rms} occurred at the beginning of the flood as well as when the ebb water depth was less than 0.20 m, which showed a clear correlation with the current velocity (Figure 6C).

The SSC at QSG was almost the same as that at KDD. The SSC ranged from 0.05–0.53 g/L with an average value of 0.21 g/L at the QSG (Figure 5A), and at the KDD it was from 0.13–0.63 g/L with an average value of 0.24 g/L (Figure 5B). However, for each tidal cycle, the SSC trend differed remarkably between the two sites. At the QSG site, the SSC was higher than 0.20 g/L for most of the study period.

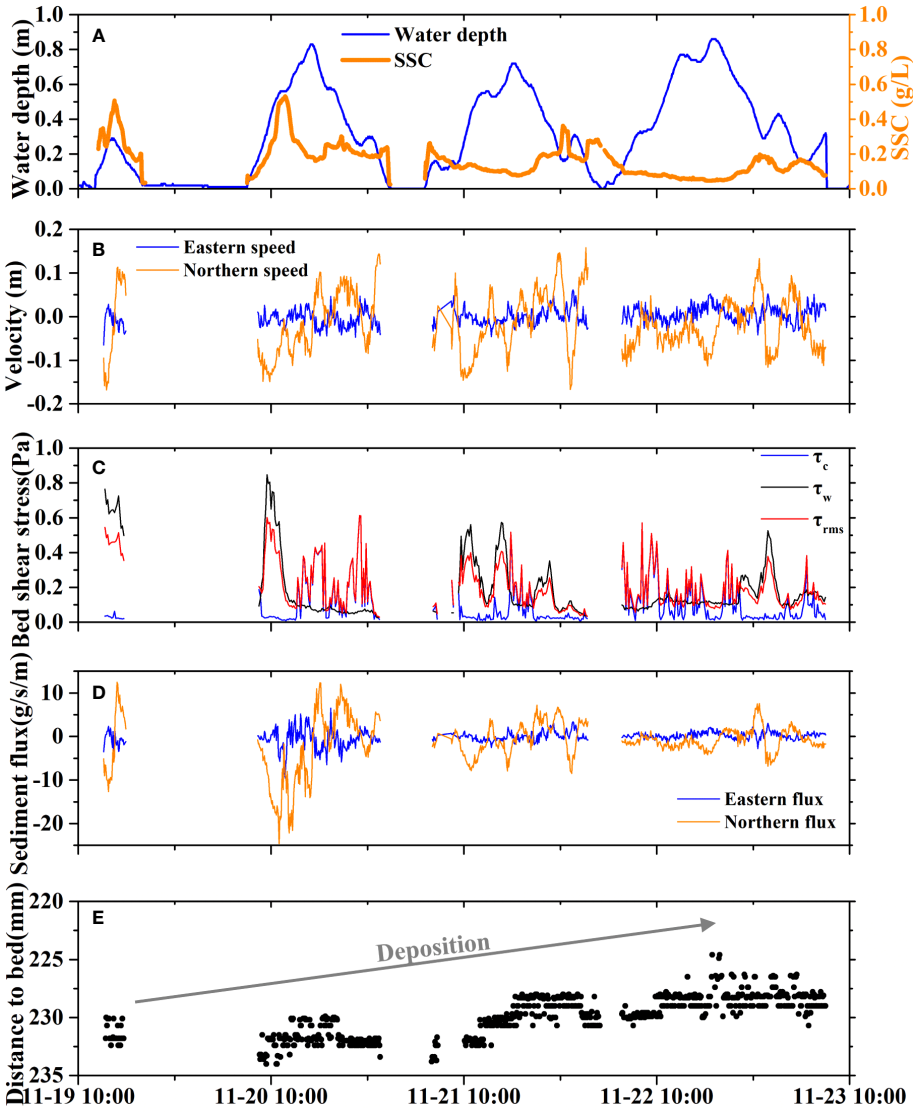

FIGURE 5
At the QSG site, time series of **(A)** tidal elevation and SSC, **(B)** current velocities at eastern and northern directions, **(C)** bed shear stress due to current (τ_c), wave (τ_w) and the combined current-wave action (τ_{cw}), **(D)** sediment fluxes at eastern and northern directions, and **(E)** bed-level change.

The peak SSCs were in phase with high water levels (>0.30 m) (Figure 5A). During Tide 3 and Tide 4, high SSC values occurred at the beginning of the flood periods. The mean SSC during the flood and the ebb tides were 0.21 g/L and 0.22 g/L, respectively (Table 1). At the KDD site, the SSC was also always higher than 0.20 g/L, but inundation was much shorter than that of the QSG site (Figure 6A). The mean SSC during the flood period and the ebb period were both 0.24 g/L (Table 1). The SSC had two peaks within a tidal cycle: before the high slack water in the flood, and near the end of the ebb. The peak SSC corresponded to high velocities, possibly owing to local erosion and sediment resuspension.

At the QSG site, the SSC showed no clear correlation with the bed shear stress (Figure 7A). The high SSC appeared at the beginning of flood periods or during high slack water when the bed shear stress was relatively low. The SSC at the KDD site followed the same trend as the bed shear stress (Figure 7B). The peak SSC clearly corresponded to high bed shear stress but with a short delay in time due to the horizontal advection.

3.3 Different sediment flux and morphological change

The sediment flux was calculated multiplying the velocity by the water depth and the SSC. As the velocity was projected along the eastern and northern directions, the sediment flux was also computed in these two directions (Figures 5D, 6D). The sediment flux at the QSG site was greater than at of the KDD site.

At the QSG site, the sediment flux in the eastern direction was smaller than that in the northern direction (Figure 5D). During floods, the tidal mean sediment flux was westward in the range of 0.54–9.00 kg/m with an average value of 3.44 kg/m, and the

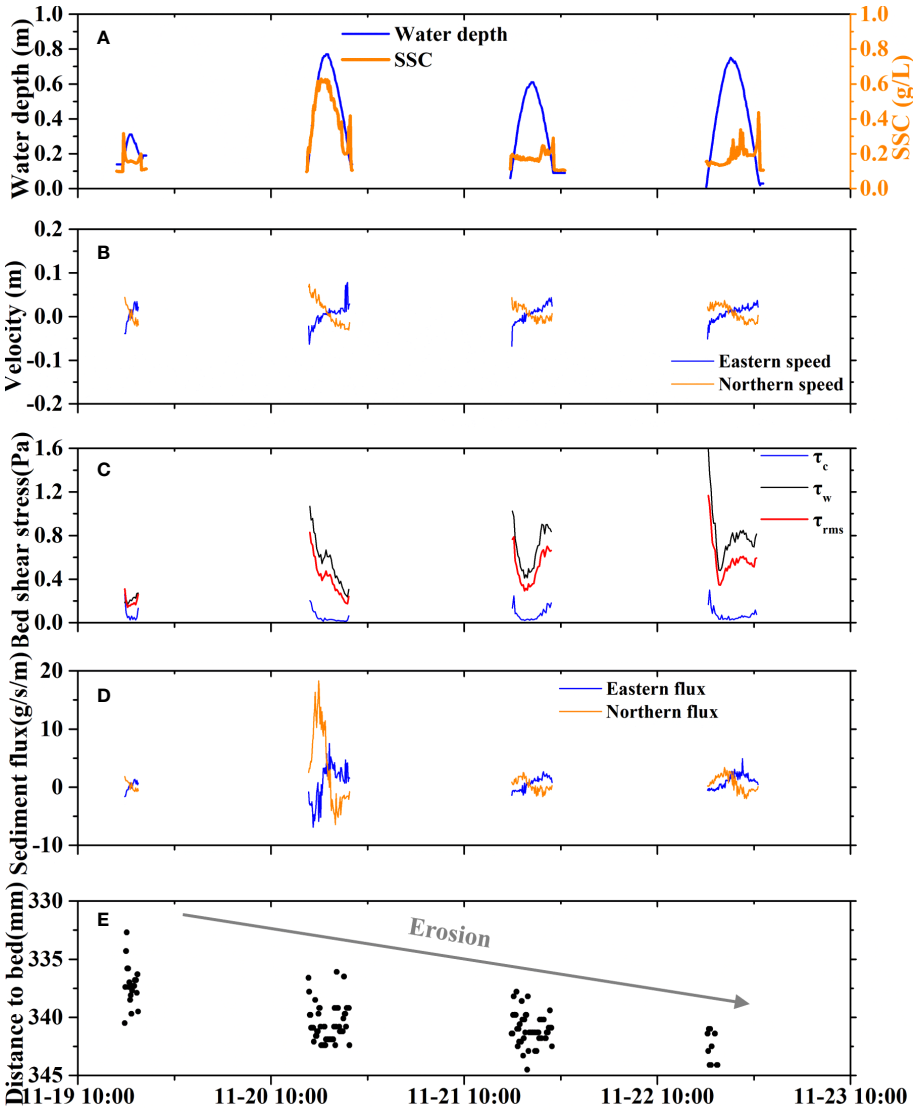

FIGURE 6
At the KDD site, time series of **(A)** tidal elevation and SSC, **(B)** current velocities at eastern and northern directions, **(C)** bed shear stress due to current (τ_c), wave (τ_w) and the combined current-wave action (τ_{cw}), **(D)** sediment fluxes at eastern and northern directions, and **(E)** bed-level change.

TABLE 1 Results of the analysis of current velocity (m/s), bed shear stress (N/m^2), and suspended sediment concentration (SSC) (g/L) at the QSG and the KDD sites.

Tides	Flood/Ebb	Current velocity Avg ± Std (m/s)		Bed shear stress Avg ± Std (N/m^2)		SSC Avg ± Std (g/L)	
		QSG	KDD	QSG	KDD	QSG	KDD
1	Flood	0.11 ± 0.04	0.03 ± 0.01	0.48 ± 0.03	0.19 ± 0.06	0.34 ± 0.08	0.16 ± 0.02
	Ebb	0.08 ± 0.02	0.02 ± 0.01	0.44 ± 0.05	0.19 ± 0.03	0.37 ± 0.09	0.15 ± 0.01
2	Flood	0.08 ± 0.04	0.04 ± 0.02	0.27 ± 0.16	0.54 ± 0.14	0.29 ± 0.13	0.50 ± 0.14
	Ebb	0.06 ± 0.03	0.03 ± 0.02	0.22 ± 0.16	0.30 ± 0.09	0.21 ± 0.03	0.39 ± 0.14
3	Flood	0.07 ± 0.04	0.02 ± 0.01	0.24 ± 0.11	0.44 ± 0.15	0.12 ± 0.03	0.17 ± 0.01
	Ebb	0.06 ± 0.04	0.02 ± 0.01	0.12 ± 0.06	0.57 ± 0.11	0.17 ± 0.07	0.20 ± 0.03
4	Flood	0.05 ± 0.02	0.03 ± 0.01	0.20 ± 0.13	0.60 ± 0.24	0.08 ± 0.01	0.14 ± 0.01
	Ebb	0.05 ± 0.03	0.02 ± 0.01	0.16 ± 0.08	0.57 ± 0.03	0.11 ± 0.05	0.22 ± 0.04

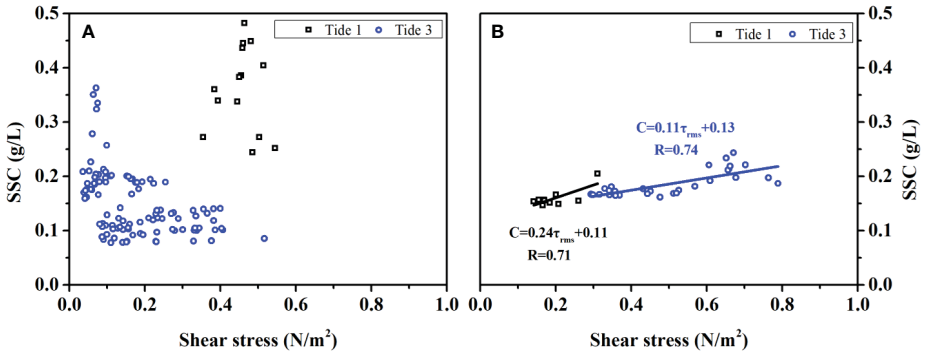

FIGURE 7
Scatterplots relating bed shear stress to SSC during Tide 1 and Tide 3 at **(A)** the QSG site, and **(B)** the KDD site.

sediment flux in the other direction was southward and greater, with an average value of 106.58 kg/m. During ebbs, the eastern sediment flux was −0.97 kg/m on average, and the northern sediment flux was 36.13 kg/m (Table 2).

At the KDD site, the sediment flux was correlated with the velocity (Figure 6D). During the flood period, the tidal mean sediment fluxes in the eastern and northern directions were -3.98 kg/m and 27.33 kg/m, respectively. During the ebb periods, the average eastern sediment flux was 16.48 kg/m, and the northern sediment flux was −6.25 kg/m (Table 2).

At the QSG site, the average net sediment flux per tidal cycle in the eastern direction was −4.23 kg/m, and −65.39 kg/m in the northern direction (Table 2), indicating that a large amount of sediment was delivered to the QSG site (Figure 8A). At the KDD site, the net sediment flux per tidal cycle in the eastern and northern directions were 13.19 kg/m and 20.77 kg/m, respectively, which indicated a moderate amount of sediment was removed from the KDD site.

The bed level change at the QSG and KDD sites displayed a clear correlation with the sediment flux. At the QSG site, the bed elevation increased by 8 mm, suggesting net deposition over the tidal cycles (Figure 5E). However, at the KDD site, the bed level decreased by 10 mm, suggesting bed erosion (Figure 6E).

4 Discussion

4.1 Different patterns of sedimentary processes

The two sites in the Yellow River Delta exhibited very different types of behavior regarding the hydrodynamics and sedimentary

TABLE 2 Statistics of the sediment flux during the flood and ebb periods, net sediment flux within a tidal cycle, average sediment flux per tidal cycle, at the QSG and KDD sites.

Tides	Flood/Ebb	QSG sediment flux (kg/m)		KDD sediment flux (kg/m)	
		East	North	East	North
1	Flood	−0.54	−40.07	−1.32	2.48
	Ebb	−6.40	33.24	2.40	−1.03
	Net	−6.94	−6.83	1.08	1.45
2	Flood	−3.51	−259.29	−12.36	82.55
	Ebb	−31.74	98.99	28.16	−21.04
	Net	−35.25	−160.30	15.80	61.51
3	Flood	−9.00	−77.75	−2.04	10.30
	Ebb	10.52	52.85	13.95	−4.10
	Net	1.52	−24.90	11.91	6.20
4	Flood	−0.68	−39.61	−0.21	14.16
	Ebb	24.42	−29.91	21.18	−0.24
	Net	23.74	−69.52	23.97	13.92
Average sediment flux per tidal cycle		−4.23	−65.39	13.19	20.77

Positive values represent eastern/northern directions and negative values represent western/southern directions.

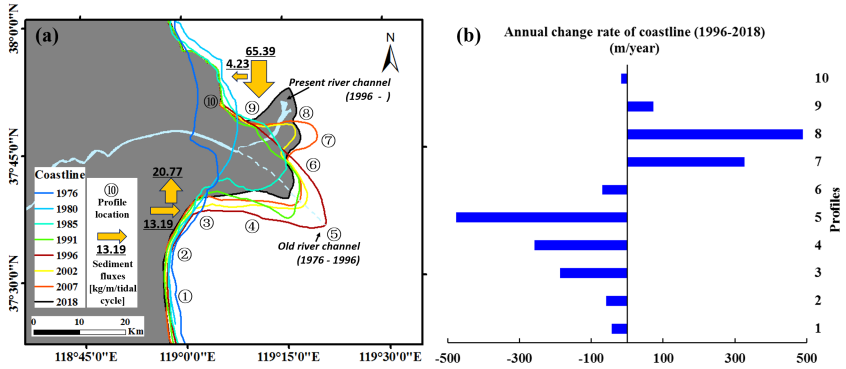

FIGURE 8
(A) Map showing the shoreline of the Yellow River Delta in different years (1976, 1980, 1985, 1991, 1996, 2002, 2007, and 2018), with the average net sediment fluxes per tidal cycle at the two sites **(A, B)** annual change rate of coastline (1996–2018) of the delta.

processes. The northern QSG tidal flat was deposited, whereas the southern KDD site eroded during the observation (Figures 5E, 6E). The two sites had similar sediment compositions (Figure 2), suggesting that the sediment source of each site was likely to be the same, both from the adjacent estuary and riverine inputs (Herrling and Winter, 2018; Pearson et al., 2020). It could be concluded that tidal and wave conditions were responsible for this difference. The northern QSG site was in a diurnal tidal environment, whereas the southern KDD site was in a mixed semi-diurnal tidal environment (Figure 9; Ji et al., 2020). As a result, the inundation period of the QSG site was much longer than that of the KDD site (Figure 4). Longer inundation times were associated with greater water depths, which promoted sedimentation on the tidal flats (Yang et al., 2008; Davis et al., 2017). Moreover, more powerful waves at the KDD site under a shallow water environment resulted in comparatively more erosion than at the QSG site (Shi et al., 2019).

Notably, at the QSG site, a high SSC occurred at the beginning of the flood period and at high slack water (Figure 5), which indicated that a large amount of sediment was transported from the adjacent sea to the tidal flat (Shi et al., 2012; Nowacki and Ganju, 2021). In contrast, the KDD site showed large temporal variations in SSC, which correlated highly with the large bed shear stress at the KDD site (Figure 6). A high-SSC environment and long slack water period provided favorable conditions for sediment settling at the QSG site, whereas a large bed shear stress led to sediment resuspension at the KDD site. Previous studies indicated that longshore currents flowed from north to south during flood tides while from south to north during ebb tides in the Yellow River Delta (Bi et al., 2010; Fan et al., 2020). The direction of the residual water mass and sediment transport was northeast at KDD and was southwest at QSG during fair weather conditions (Fan et al., 2020; Ji et al., 2022), which agreed with the results of the net sediment fluxes at the two sites in this study.

In this study, we proposed an integrated conceptual model to describe the sedimentary processes at the two sites (Figure 10). At the QSG site with diurnal tides, the sediment from the adjacent estuarine water was delivered to the tidal flat; additionally, it was resuspended due to high bed shear stress, leading to rich sediment supply and a high SSC environment. Combined with a relatively high-water level, most of the sediment settled and deposited (Figure 10A). At the KDD site, with mixed semi-diurnal tides, relatively strong wave activity, combined with shallow water, resulted in high bed shear stress and sediment erosion from the bed. Unlike the QSG site, which was always submerged, the KDD site was predominantly eroded during a short period of inundation when the bed shear stress was high. The eroded sediment was transported to the subtidal area and the adjacent estuarine water, leading to erosion at the KDD site (Figure 10B).

FIGURE 9
Different types of tides in the Yellow River Delta (modified after Ji et al., 2020).

4.2 Determinants of asymmetric evolution

Previous studies have reported that estuarine tidal flat evolution was jointly influenced by the fluvial sediment supply, tidal currents, waves, and vegetation (Temmerman et al., 2003; Mariotti and Fagherazzi, 2013; Xie et al., 2021). The fluvial sediment supply affected tidal flat evolution by controlling sediment availability (Yang et al., 2011b; Nittrouer et al., 2021; Ji et al., 2022). A larger

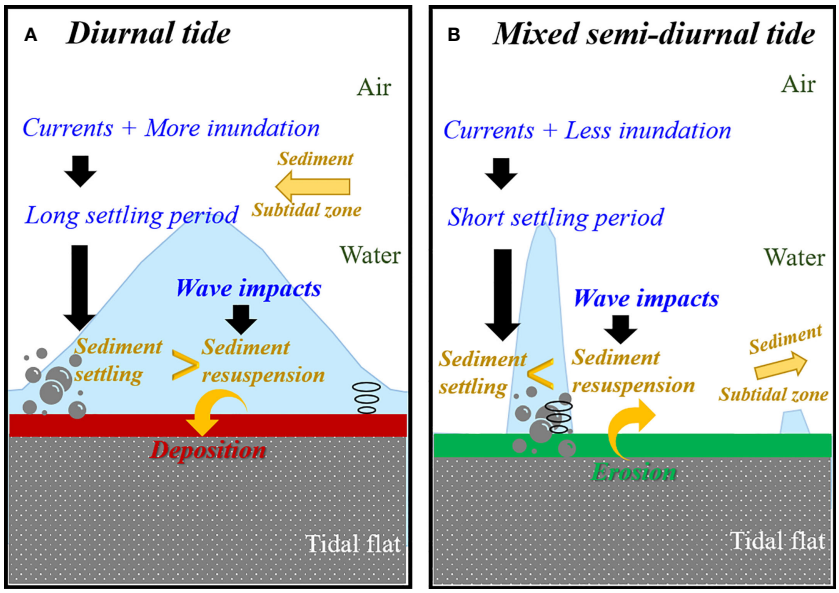

FIGURE 10
Conceptual models for different sedimentary processes in the **(A)** diurnal-tide environment and **(B)** mixed semi-tide environment.

riverine sediment input enhanced sediment availability, leading to delta progradation and associated tidal flat accretion (Blum and Roberts, 2012; Bi et al., 2021). In this study, the fluvial sediment supply was not a determinant factor for the asymmetric evolution in the Yellow River Delta. The river channel of the delta was along the northwest-southeast direction before 1996 and was closer to the KDD site (Figure 1). After 1996, the river shifted to the present channel position, which was in the northeast–southwest direction and closer to the QSG site. If the fluvial sediment supply was the dominant factor, the KDD site would have accumulated and deposited sediment between 1976 and 1996. However, coastline changes indicated that the southern tidal flat of the delta was eroded and retreated between 1976 and 1996 (Figure 8). These results suggested that the fluvial sediment supply was not directly responsible for the contrasting evolution of the Yellow River Delta. Previous studies have reported that local sediment availability had a direct positive impact on tidal flat evolution (Kirwan and Megonigal, 2013; Schuerch et al., 2014; Maan et al., 2019). Besides riverine sediment supply, local sediment availability for a tidal flat was also influenced by local hydrodynamics, plant growth, and human modification (Friedrichs, 2011; Roman, 2017; Xie et al., 2018b). In this study, we chose to perform the measurements in November, when the fluvial sediment flux from the Yellow River was low. In this study, we chose to perform the measurements in November, when the fluvial sediment flux from the Yellow River was low. During the study period, the different tidal conditions in the Yellow River Delta, were the principal factor in controlling the local sediment availability. The diurnal-tidal environment in the northern part of the delta enhanced sediment import from the adjacent estuarine water and increased the inundation time of tidal flats (Figure 10A). The tidal conditions provided favorable environment for sediment settling, which helped capture sediment on tidal flats (van Proosdij et al., 2006; Xie et al., 2018b). The mixed semi-diurnal tidal environment in the southern part of the delta led to a shorter inundation period compared with the northern part, thus tidal flats were unlikely to trap sediment (Figure 10B). The difference in tidal conditions might explain why the asymmetric evolution in the Yellow River Delta did not respond to the river channel shift.

The second influential factor in tidal flat evolution was wave activity. The bed shear stress (τ_{rms}) was important to sedimentary processes of tidal flats. Wave-driven sediment resuspension and transport, interacted with sediment transport driven by currents, always controlled sediment erosion and deposition on tidal flats (van Rijn, 1993; Green and Coco, 2014). The KDD tidal flat, which was open to the sea, was more likely to experience stronger wave energy than the sheltered QSG tidal flat. Moreover, waves played a vital role in river delta progradation and channel avulsion (Nienhuis et al., 2016; Gao et al., 2020). In some cases, waves controlled channel orientation and, therefore, asymmetric growth by wave-driven bypassing sediment flux (Nienhuis et al., 2016).

The third significant factor was vegetation. Vegetation, which attenuated wave energy and enhanced sediment trapping, also played an important role in the tidal flat evolution (Yang et al., 2008). The vegetation at the QSG site was *Spartina alterniflora* which had been proven to be effective in trapping sediment on tidal flats (Yuan et al., 2011; Angelini et al., 2018), whereas the KDD site was almost bare without vegetation (Figure 11). Different vegetation condition was also the impact factor in determining the contrasting evolution of the Yellow River Delta.

4.3 Management implications

Coastal regions are highly sensitive to change, caused by natural variations as well as human modifications. This includes the

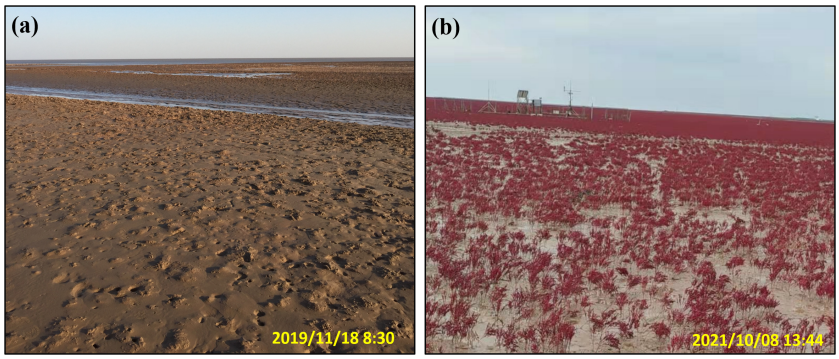

FIGURE 11
Photographs showing **(A)** the bare flat in the southern KDD site in 2019 and **(B)** the same location after *Suaeda salsa* restoration and colonization in 2021.

increasing changes in climate, specifically rising sea-levels and extreme weather events. Regional water and sediment management are urgently required to minimize the effects of such risks (Kirwan and Megonigal, 2013; Syvitski et al., 2022). Tidal flats are important components of river deltas and usually act as sediment sources for both salt marshes and estuarine waters (Friedrichs, 2011; Donatelli et al., 2018). For effective coastal protection and management, a better understanding of sedimentary processes on tidal flats, and their determinants, is required (Schuerch et al., 2014). The determinants of these tidal flat sedimentary processes vary in different estuarine environments. For example, storm-associated waves and storm surges dominated tidal flat sedimentation in an open-coast tidal flat in the south-western Korea (Yang et al., 2005). However, for the Kapellebank tidal flat in the Netherlands, storm events were infrequent and therefore did not affect the long-term morphodynamics of the tidal flat; while small wind waves had a significant stabilizing effect on tidal flat evolution (Maan et al., 2018). Field measurements also confirmed the ability of the tidal flat system to quickly recover from storms (Xie et al., 2017). Flow asymmetry and mud properties were also reported to influence tidal flat sedimentation (van Maren and Winterwerp, 2013). Moreover, local sediment availability was considered to have strong impacts on the intertidal environment in the Delaware bay and the Yangtze Estuary (Stammermann and Piasecki, 2012; Xie et al., 2018b).

The sediment composition and mud properties were almost identical at the two sites studied. The influence of the fluvial sediment supply could be omitted during the study period. The results of this study suggested that tidal conditions, waves, and local sediment availability were the main determinants of the asymmetric evolution in the Yellow River Delta. The different tidal condition was the most important impact factor, because it formed long inundation period and reduced the wave effect at the QSG site. The tidal environment made the QSG site quite suitable for sediment settling and deposition. Richer local sediment availability in the northern part might also have a positive effect on the depositional process at the QSG site compared to that at the KDD site. Owing to the large decrease in fluvial sediment supply, tidal flats in the Yellow River Delta experienced severe erosion and retreat (Wang et al., 2017). Moreover, it should be noted that the above sedimentary patterns of the two contrasting tidal flats were concluded under fair weather conditions, which appeared different during storms. Storms greatly affected longshore currents, changed the direction and enhanced the magnitude of residual water mass and sediment flux in the Yellow River Delta. For example, the residual currents were transported toward the northeast at KDD under fair weather conditions. Affected by the northerly storm, the residual transport of water flowed southward (Fan et al., 2020). Moreover, the trends of sediment transport under the combined influence of river-tide-wave dynamics, also differed from those under river-tide dynamics (Ji et al., 2022), indicating that storms could sharply alter local hydrodynamics, sediment availability, and sedimentary processes of tidal flats within a short period of time.

Considering the different tidal conditions in the northern and southern parts of the Yellow River Delta, solutions to protect estuarine tidal flats might be different. In the northern part, if sediment availability could be enhanced, additional sediment could be transported to tidal flats and settle easily due to the diurnal tide environment. For the southern part, the inundation period was quite short, and the wave effect was relatively high due to the shallow water. Vegetation restoration, which could attenuate waves and increase the capability to trap more sediment, would be a good solution to avoid continuing erosion in this area. The southern part of the Yellow River Delta has already implemented a similar solution with the establishment of *Suaeda salsa* to protect tidal flats (Figure 11).

5 Conclusions

In this study, we examined the hydrodynamics, sediment transport dynamics, and morphological changes at two micro-tidal sites in the Yellow River Delta based on field measurements. We also observed distinctive tidal flat evolution patterns of the two sites, which were ascribed to the combined effects of tidal forcing and wave climate. The field study showed that the inundation period of the northern QSG site was much longer than that of the southern KDD site. At the QSG site, a landward sediment flux led to

deposition on the tidal flats. At the KDD site, the sediment was resuspended and eroded locally because of the larger bed shear stress and short submerged period. The results suggested that tidal conditions, waves, and local sediment availability were the main determinants of the contrasting evolution in the Yellow River Delta. The SSC and flow asymmetries determined the intertidal sedimentary process in the absence of strong waves.

This study highlighted the profound hydro-morphodynamic effect of tidal conditions on asymmetric tidal flat evolution, which shed light on coastal protection and management. The field results indicated that enhancing sediment availability would be favorable for more sedimentation and deposition in the northern part of the Yellow River Delta. In the southern part, vegetation restoration could attenuate waves and was beneficial for preventing tidal flats from continuing erosion.

Data availability statement

The raw data supporting the conclusions of this article will be made available by the authors, without undue reservation.

Author contributions

WX: Writing – original draft, Writing – review and editing. JS: Conceptualization, Data curation, Writing – review and editing. LG: Writing – review and editing. FX: Writing – review and editing. XW: Supervision, Writing – review and editing. HJ: Data curation, Visualization, Writing – review and editing. YF: Methodology, Validation, Writing – review and editing. ZW: Supervision, Writing – review and editing. QH: Supervision, Writing – review and editing.

Funding

This work is financially supported by the National Natural Science Foundation of China (Nos. U2243207, 42276217, 51909101, U2040216). Financial support from Ministry of Science and Technology of China (No. 2016YFE0133700), and Royal Netherlands Academy of Arts and Sciences (KNAW) (No. PSA-SA-E-02) is also acknowledged. This project is also funded by the Yangtze Delta Estuarine Wetland Ecosystem Observation and Research Station, Ministry of Education & Shanghai Science and Technology Committee (ECNU-YDEWS-2022).

Acknowledgments

We would like to thank Zhonghao Zhao and Shang Yu for their assistance in the field work.

Conflict of interest

The authors declare that the research was conducted in the absence of any commercial or financial relationships that could be construed as a potential conflict of interest.

Publisher's note

All claims expressed in this article are solely those of the authors and do not necessarily represent those of their affiliated organizations, or those of the publisher, the editors and the reviewers. Any product that may be evaluated in this article, or claim that may be made by its manufacturer, is not guaranteed or endorsed by the publisher.

References

Allen, J. R. L. (2000). Morphodynamics of Holocene salt marshes: a review sketch from the Atlantic and Southern North Sea coasts of Europe. *Quaternary Sci. Rev.* 19 (12), 1155–1231. doi: 10.1016/S0277-3791(99)00034-7

Andersen, T. J., Fredsoe, J., and Pejrup, M. (2007). *In situ* estimation of erosion and deposition thresholds by Acoustic Doppler Velocimeter (ADV). *Estuarine Coast. Shelf Sci.* 75 (3), 327–336. doi: 10.1016/j.ecss.2007.04.039

Angelini, C., van Montfrans, S. G., Hensel, M., He, Q., and Silliman, B. R. (2018). The importance of an underestimated grazer under climate change: how crab density, consumer competition, and physical stress affect salt marsh resilience. *Oecologia* 187 (1), 205–217. doi: 10.1007/s00442-018-4112-8

Bi, N., Wang, H., Wu, X., Saito, Y., Xu, C., and Yang, Z. (2021). Phase change in evolution of the modern Huanghe (Yellow River) Delta: Process, pattern, and mechanisms. *Mar. Geology* 437, 106516. doi: 10.1016/j.margeo.2021.106516

Bi, N., Yang, Z., Wang, H., Hu, B., and Ji, Y. (2010). Sediment dispersion pattern off the present Huanghe (Yellow River) subdelta and its dynamic mechanism during normal river discharge period. *Estuarine Coast. Shelf Sci.* 86 (3), 352–362. doi: 10.1016/j.ecss.2009.06.005

Blum, M. D., and Roberts, H. H. (2012). The mississippi delta region: past, present, and future. *Annu. Rev. Earth Planetary Sci.* 40 (1), 655–683. doi: 10.1146/annurev-earth-042711-105248

Bouma, T. J., Friedrichs, M., van Wesenbeeck, B. K., Temmerman, S., Graf, G., and Herman, P. M. J. (2009). Density-dependent linkage of scale-dependent feedbacks: a flume study on the intertidal macrophyteSpartina anglica. *Oikos* 118 (2), 260–268. doi: 10.1111/j.1600-0706.2008.16892.x

Bouma, T. J., van Belzen, J., Balke, T., van Dalen, J., Klaassen, P., Hartog, A. M., et al. (2016). Short-term mudflat dynamics drive long-term cyclic salt marsh dynamics. *Limnology Oceanography* 61 (6), 2261–2275. doi: 10.1002/lno.10374

D'Alpaos, A., and Marani, M. (2016). Reading the signatures of biologic–geomorphic feedbacks in salt-marsh landscapes. *Adv. Water Resour.* 93, 265–275. doi: 10.1016/j.advwatres.2015.09.004

Davis, J., Currin, C., and Morris, J. T. (2017). Impacts of fertilization and tidal inundation on elevation change in microtidal, low relief salt marshes. *Estuaries Coasts* 40, 1677–1687. doi: 10.1007/s12237-017-0251-0

Donatelli, C., Ganju, N. K., Zhang, X., Fagherazzi, S., and Leonardi, N. (2018). Salt marsh loss affects tides and the sediment budget in shallow bays. *J. Geophysical Research: Earth Surface* 123 (10), 2647–2662. doi: 10.1029/2018JF004617

Fan, Y., Chen, S., Pan, S., and Dou, S. (2020). Storm-induced hydrodynamic changes and seabed erosion in the littoral area of Yellow River Delta: A model-guided mechanism study. *Continental Shelf Res.* 205, 104171. doi: 10.1016/j.csr.2020.104171

Friedrichs, C. T. (2011). Tidal flat morphodynamics: A synthesis. In *Treatise on Estuarine and Coastal Science, Estuarine and Coastal Geology and Geomorphology*; J. D. Hansom and B. W. Fleming, Eds. (Amsterdam: Elsevier) 137–170.

Gao, W., Nienhuis, J., Nardin, W., Wang, Z. B., Shao, D., Sun, T., et al. (2020). Wave controls on deltaic shoreline-channel morphodynamics: insights from a coupled model. *Water Resour. Res.* 56 (9), e2020WR027298. doi: 10.1029/2020WR027298

Green, M. O., and Coco, G. (2014). Review of wave-driven sediment resuspension and transport in estuaries. *Rev. Geophysics* 52 (1), 77–117. doi: 10.1002/2013RG000437

Herrling, G., and Winter, C. (2018). Tidal inlet sediment bypassing at mixed-energy barrier islands. *Coast. Eng.* 140, 342–354. doi: 10.1016/j.coastaleng.2018.08.008

IPCC (2021). "Summary for policymakers," in *Climate Change 2021: The Physical Science Basis. Contribution of Working Group I to the Sixth Assessment Report of the Intergovernmental Panel on Climate Change*. Eds. V. Masson-Delmotte, P. Zhai, A. PIrani, S. L. Connors, C. Péan, S. Berger, N. Caud, Y. Chen, L. Goldfarb, M. I. Gomis, M. Huang, K. Leitzell, E. Lonnoy, J. B. R. Matthews, T. K. Maycock, T. Waterfield, O. Yelekçi, R. Yu and B. Zhou (Cambridge: Cambridge University Press).

Ji, H., Chen, S., Pan, S., Xu, C., Tian, Y., Li, P., et al. (2022). Fluvial sediment source to sink transfer at the Yellow River Delta: Quantifications, causes, and environmental impacts. *J. Hydrology* 608, 127622. doi: 10.1016/j.jhydrol.2022.127622

Ji, H., Pan, S., and Chen, S. (2020). Impact of river discharge on hydrodynamics and sedimentary processes at Yellow River Delta. *Mar. Geology* 425, 106210. doi: 10.1016/j.margeo.2020.106210

Kirwan, M. L., and Megonigal, J. P. (2013). Tidal wetland stability in the face of human impacts and sea-level rise. *Nature* 504 (7478), 53–60. doi: 10.1038/nature12856

Leuven, J. R. F. W., Pierik, H. J., Vegt, M. V. D., Bouma, T. J., and Kleinhans, M. G. (2019). Sea-level-rise-induced threats depend on the size of tide-influenced estuaries worldwide. *Nat. Climate Change* 9 (12), 986–992. doi: 10.1038/s41558-019-0608-4

Li, H., and Yang, S. L. (2009). Trapping effect of tidal marsh vegetation on suspended sediment, Yangtze Delta. *J. Coast. Res.* 25 (4), 915–924. doi: 10.2112/08-1010.1

Liu, B., Cai, T., Chen, Y., Yuan, B., Wang, R., and Xiao, M. (2022). Sediment dynamic changes induced by the presence of a dyke in a Scirpus mariqueter saltmarsh. *Coast. Eng.* 174, 104119. doi: 10.1016/j.coastaleng.2022.104119

Maan, D. C., Prooijen, B. C. V., and Wang, Z. B. (2019). Progradation speed of tide-dominated tidal flats decreases stronger than linearly with decreasing sediment availability and linearly with sea level rise. *Geophysical Res. Lett* 46 (1), 262–271. doi: 10.1029/2018GL079933

Maan, D. C., Prooijen, B. C., Zhu, Q., and Wang, Z. B. (2018). Morphodynamic feedback loops control stable fringing flats. *J. Geophysical Research: Earth Surface* 123 (11), 2993–3012. doi: 10.1029/2018JF004659

Mariotti, G., and Fagherazzi, S. (2013). A two-point dynamic model for the coupled evolution of channels and tidal flats. *J. Geophysical Research: Earth Surface* 118 (3), 1387–1399. doi: 10.1002/jgrf.20070

Mariotti, G., and Fagherazzi, S. (2011). Asymmetric fluxes of water and sediments in a mesotidal mudflat channel. *Cont. Shelf Res.* 31 (1), 23–36. doi: 10.1016/j.csr.2010.10.014

Mariotti, G., Fagherazzi, S., Wiberg, P. L., McGlathery, K. J., Carniello, L., and Defina, A. (2010). Influence of storm surges and sea level on shallow tidal basin erosive processes. *J. Geophysical Res.* 115 (C11), 0148–0227. doi: 10.1029/2009JC005892

Nienhuis, J. H., Ashton, A. D., and Giosan, L. (2016). Littoral steering of deltaic channels. *Earth Planetary Sci. Lett.* 453, 204–214. doi: 10.1016/j.epsl.2016.08.018

Nittrouer, C. A., DeMaster, D. J., Kuehl, S. A., Figueiredo, A. J., Sternberg, R. W., Faria, L., et al. (2021). Amazon sediment transport and accumulation along the continuum of mixed fluvial and marine processes. *Annu. Rev. Mar. Sci* 13, 501–536. doi: 10.1146/annurev-marine-010816-060457

Nowacki, D. J., and Ganju, N. K. (2021). Sediment dynamics of a divergent bay–marsh complex. *Estuaries Coasts* 44 (5), 1216–1230. doi: 10.1007/s12237-020-00855-5

Pearson, S. G., Prooijen, B. C., Elias, E. P. L., Vitousek, S., and Wang, Z. B. (2020). Sediment connectivity: A framework for analyzing coastal sediment transport pathways. *J. Geophysical Research: Earth Surface* 125 (10), e2020JF005595. doi: 10.1029/2020JF005595

Pope, N. D., Widdows, J., and Brinsley, M. D. (2006). Estimation of bed shear stress using the turbulent kinetic energy approach – A comparison of annular flume and field data. *Continental Shelf Res.* 26 (8), 959–970. doi: 10.1016/j.csr.2006.02.010

Roman, C. T. (2017). Salt marsh sustainability: challenges during an uncertain future. *Estuaries Coasts* 40, 711–716. doi: 10.1007/s12237-016-0149-2

Schuerch, M., Dolch, T., Reise, K., and Vafeidis, A. T. (2014). Unravelling interactions between salt marsh evolution and sedimentary processes in the Wadden Sea (southeastern North Sea). *Prog. Phys. Geogr.* 38 (6), 691–715. doi: 10.1177/0309133314548746

Shi, B., Cooper, J. R., Li, J., Yang, Y., Yang, S. L., Luo, F., et al. (2019). Hydrodynamics, erosion and accretion of intertidal mudflats in extremely shallow waters. *J. Hydrology* 573, 31–39. doi: 10.1016/j.jhydrol.2019.03.065

Shi, B. W., Yang, S. L., Wang, Y. P., Bouma, T. J., and Zhu, Q. (2012). Relating accretion and erosion at an exposed tidal wetland to the bottom shear stress of combined current–wave action. *Geomorphology* 138 (1), 380–389. doi: 10.1016/j.geomorph.2011.10.004

Soulsby, R. (1997). *Dynamics of marine sands* (Thomas Telford Publishing, London, The United Kingdom: A manual for practical applications).

Soulsby, R., and Clarke, S. (2005). *Bed shear-stresses Under Combined Waves and Currents on Smooth and Rough Beds* (Wallingford: HR Wallingford).

Spencer, T., Schuerch, M., Nicholls, R. J., Hinkel, J., Lincke, D., Vafeidis, A. T., et al. (2016). Global coastal wetland change under sea-level rise and related stresses: The DIVA Wetland Change Model. *Global Planetary Change* 139, 15–30. doi: 10.1016/j.gloplacha.2015.12.018

Stammermann, R., and Piasecki, M. (2012). Influence of sediment availability, vegetation, and sea level rise on the development of tidal marshes in the delaware bay: A review. *J. Coast. Res.* 285, 1536–1549. doi: 10.2112/JCOASTRES-D-11-00143.1

Stapleton, K. R., and Huntley, D. A. (1995). Seabed stress determinations using the inertial dissipation method and the turbulent kinetic energy method. *Earth Surface Processes Landforms* 20 (9), 807–815. doi: 10.1002/esp.3290200906

Stokes, G. G. (1847). On the theory of oscillatory waves. *Trans. Cambridge Philos. Soc.* 8, 441–455. doi: 10.1017/CBO9780511702242.013

Syvitski, J., Ángel, J. R., Saito, Y., Overeem, I., Vörösmarty, C. J., Wang, H., et al. (2022). Earth's sediment cycle during the Anthropocene. *Nat. Rev. Earth Environ.* 3 (3), 179–196. doi: 10.1038/s43017-021-00253-w

Syvitski, J. P. M., Kettner, A. J., Overeem, I., Hutton, E. W. H., Hannon, M. T., Brakenridge, G. R., et al. (2009). Sinking deltas due to human activities. *Nat. Geosci.* 2 (10), 681–686. doi: 10.1038/ngeo629

Temmerman, S., Bouma, T. J., Govers, G., and Lauwaet, D. (2005). Flow paths of water and sediment in a tidal marsh: Relations with marsh developmental stage and tidal inundation height. *Estuaries* 28 (3), 338–352. doi: 10.1007/BF02693917

Temmerman, S., Govers, G., Wartel, S., and Meire, P. (2003). Spatial and temporal factors controlling short-term sedimentation in a salt and freshwater tidal marsh, Scheldt estuary, Belgium, SW Netherlands. *Earth Surface Processes Landforms* 28 (7), 739–755. doi: 10.1002/esp.495

Temmerman, S., Meire, P., Bouma, T. J., Herman, P., and Ysebaert, T. (2013). Ecosystem-based coastal defence in the face of global change. *Nature* 504 (7478), 79–83. doi: 10.1038/nature12859

van der Wal, D., and Pye, K. (2004). Patterns, rates and possible causes of saltmarsh erosion in the Greater Thames area (UK). *Geomorphology* 61 (3-4), 373–391. doi: 10.1016/j.geomorph.2004.02.005

van der Wegen, M. (2013). Numerical modeling of the impact of sea level rise on tidal basin morphodynamics. *J. Geophysical Research: Earth Surface* 118 (2), 447–460. doi: 10.1002/jgrf.20034

van Maren, D. S., and Winterwerp, J. C. (2013). The role of flow asymmetry and mud properties on tidal flat sedimentation. *Continental Shelf Res.* 60, S71–S84. doi: 10.1016/j.csr.2012.07.010

van Proosdij, D., Ollerhead, J., and Davidson-Arnott, R. G. D. (2006). Seasonal and annual variations in the volumetric sediment balance of a macro-tidal salt marsh. *Mar. Geology* 225 (1-4), 103–127. doi: 10.1016/j.margeo.2005.07.009

van Rijn, L. C. (1993). *Principles of Sediment Transport in Rivers, Estuaries and Coastal Seas* (Amsterdam: Aqua Publications).

Wang, Z. B., Elias, E. P. L., van der Spek, A. J. F., and Lodder, Q. J. (2018). Sediment budget and morphological development of the Dutch Wadden Sea: impact of accelerated sea-level rise and subsidence until 2100. *Netherlands J. Geosciences* 97 (3), 183–214. doi: 10.1017/njg.2018.8

Wang, H., Wu, X., Bi, N., Li, S., Yuan, P., Wang, A., et al. (2017). Impacts of the dam-orientated water-sediment regulation scheme on the lower reaches and delta of the Yellow River (Huanghe): A review. *Global Planetary Change* 157, 93–113. doi: 10.1016/j.gloplacha.2017.08.005

Xie, W., He, Q., Wang, X., Guo, L., and Zhang, K. (2018a). Role of mudflat-creek sediment exchanges in intertidal sedimentary processes. *J. Hydrology* 567, 351–360. doi: 10.1016/j.jhydrol.2018.10.027

Xie, W., He, Q., Zhang, K., Guo, L., Wang, X., and Shen, J. (2018b). Impacts of human modifications and natural variations on short-term morphological changes in estuarine tidal flats. *Estuaries Coasts* 41 (5), 1253–1267. doi: 10.1007/s12237-017-0352-9

Xie, W., He, Q., Zhang, K., Guo, L., Wang, X., Shen, J., et al. (2017). Application of terrestrial laser scanner on tidal flat morphology at a typhoon event timescale. *Geomorphology* 292, 47–58. doi: 10.1016/j.geomorph.2017.04.034

Xie, W., Wang, X., Guo, L., He, Q., Dou, S., and Yu, X. (2021). Impacts of a storm on the erosion process of a tidal wetland in the Yellow River Delta. *CATENA* 205, 105461. doi: 10.1016/j.catena.2021.105461

Yang, B., Dalrymple, R., and Chun, S. S. (2005). Sedimentation on a wave-dominated, open-coast tidal flat, south-western Korea: Summer tidal flat - Winter shoreface. *Sedimentology* 52, 235–252. doi: 10.1111/j.1365-3091.2004.00692.x

Yang, Z., Ji, Y., Bi, N., Lei, K., and Wang, H. (2011a). Sediment transport off the Huanghe (Yellow River) delta and the adjacent Bohai Sea in winter and seasonal comparison. *Estuarine Coast. Shelf Sci.* 93, 173–181. doi: 10.1016/j.ecss.2010.06.005

Yang, S. L., Li, H., Ysebaert, T., Bouma, T. J., Zhang, W. X., Wang, Y. Y., et al. (2008). Spatial and temporal variations in sediment grain size in tidal wetlands, Yangtze Delta: On the role of physical and biotic controls. *Estuarine Coast. Shelf Sci.* 77 (4), 657–671. doi: 10.1016/j.ecss.2007.10.024

Yang, S. L., Milliman, J. D., Li, P., and Xu, K. (2011b). 50,000 dams later: Erosion of the Yangtze River and its delta. *Global Planetary Change* 75 (1-2), 14–20. doi: 10.1016/j.gloplacha.2010.09.006

Yuan, L., Zhang, L., Xiao, D., and Huang, H. (2011). The application of cutting plus waterlogging to control Spartina alterniflora on saltmarshes in the Yangtze Estuary, China. *Estuarine Coast. Shelf Sci.* 92 (1), 103–110. doi: 10.1016/j.ecss.2010.12.019

Zhu, C., Guo, L., Maren, D. S., Tian, B., Wang, X., He, Q., et al. (2019). Decadal morphological evolution of the mouth zone of the Yangtze Estuary in response to human interventions. *Earth Surface Processes Landforms* 44 (12), 2319–2332. doi: 10.1002/esp.4647

Zhu, Q., van Prooijen, B. C., Wang, Z. B., Ma, Y. X., and Yang, S. L. (2016). Bed shear stress estimation on an open intertidal flat using in *situ* measurements. *Estuarine Coast. Shelf Sci.* 182, 190–201. doi: 10.1016/j.ecss.2016.08.028